Journal of Posthumanism
2025
Volume: 5, No: 7, pp. 1740–1754
ISSN: 2634-3576 (Print) | ISSN 2634-3584 (Online)
posthumanism.co.uk

DOI: https://doi.org/10.63332/joph.v5i7.2962

Correlation of Mechanical Parameters in Diatomaceous Soils Using Image Analysis and Digital Processing

Daniel Zuluaga-Astudillo[1], Carlos José Slebi-Acevedo[2], Juan Carlos Ruge[3]

Abstract

In the state-of-the-art, no studies are recognized regarding analyzing or processing images in diatomaceous soils for their subsequent relationship with mechanical parameters. These soils report responses and behaviors that are unusual and distant from conventional soil mechanics. This research included a diatomaceous soil of Colombian origin with cylindrical particles, in which unconfined compression, direct shear, and oedometric compression tests were carried out, and Scanning Electron Microscopy images were obtained. Analysis techniques and filters (Binarization, Voronoi, LUT) were applied to these observations. This research aims to determine if, from the images and the mechanical response results, some correlation can be established that subsequently serves as a predictive tool for the behaviour of this type of soil. The geotechnical response values are based on the study variables (diatomaceous soil content and deterioration cycles). Proportional trends that are almost linear in behaviour are identified between test values. The results of final void ratio, cohesion (kg/cm2), and strain at failure (%) obtained through laboratory tests and those calculated from image analysis are presented. A multivariate analysis was performed, and a quantitative image-based index was proposed to correlate cohesion parameters, friction angle, undrained shear strength, and strain at failure.

Keywords: *Correlation, Mechanical Parameters, Diatomaceous, Digital, Soils*

Introduction

The application of Artificial Intelligence and Image Processing Methods is becoming more frequent in civil engineering studies, whether in the description of physical properties of materials or the prediction of mechanical responses of samples. These aspects are supported in photographic captures. This initiative is motivated by the time and cost reduction that an image analysis exposes comparatively with a conventional laboratory test, serves to understand the origin of the physical response of a material at micro and nano scales, and helps to quantify and internalize concepts regarding the organization of particles within a medium. For the specific case of applications in geotechnical engineering, image processing techniques have recently been implemented in research lines such as:

- Reconstruction of rock and soil particles with irregular morphometric conditions and various sizes by applying grayscales, element extraction, and color reassignment [1].

[1] Programa de Diseño y Construcción de Vías y Aeropistas, Escuela de Ingenieros Militares.
Ejército de Colombia, Bogotá 111611, Colombia, Email: est.daniel.zuluaga@unimilitar.edu.co, daniel.zuluaga@esing.edu.co
[2] Programa de Doctorado en Ingeniería, Universidad Militar Nueva Granada, Bogotá 110111, Colombia, juan.ruge@unimilitar.edu.co
[3] PhD Program in Engineering, Universidad Militar Nueva Granada, Bogotá 110111, Colombia, Email: juan.ruge@unimilitar.edu.co

- Using soil spectral libraries (SSLs) based on visible-near infrared images to predict organic carbon (SOC). The models showed good accuracy and allowed a detailed characterization of the spatial distribution of SOC [2].
- The surface water content (SSWC) effect on soil images was studied. A multi-Gaussian (MGF) color feature extraction method was introduced to mitigate possible interferences. Color, texture, and proportion features and their relationship to SSWC were considered in the images. Results provided a non-contact monitoring method, proper in studies on seepage in porous media and water migration in unsaturated soils [3].
- The tensile strength of unsaturated clayey soils and their corresponding deformation were determined using particle image velocimetry (PIV) and digital image correlation (DIC) techniques. The location and direction of tensile fracture in the soil samples were predetermined by using the strain concentration [4].
- The description of the particle shape and the image acquisition system was assessed. Ref. [5] analyzed the relationship between the particle shape and the mechanical properties of granular soil, considering that the geometry significantly affects the macro mechanical behaviour, especially when the sphericity, roundness, and roughness are altered.
- Sand, silt, and clay contents in soil samples using near-infrared NIR and image fusion data based on a convolutional neural network (CNN) model. For the predictive model, preprocessing methods, image types, and sizes were optimized, and the performance of the CNN model was improved using a small amount of data. The proposed CNN using NIR and Image Fusion data accurately predicted silt and clay fractions [6].
- Advances in smartphone-based soil characterization. This technology has transformed traditional soil analysis methods. Methodologies used in soil image processing were examined, covering aspects such as image acquisition, segmentation, color space conversion, and feature extraction, facilitating the development of predictive models for soil attributes. Challenges were identified considering variability in illumination, moisture content, and device limitations [7].
- A prototype machine was developed to take images in controlled environments (light intensity, distance, and dry conditions) to analyze soil texture. Each sample was defined according to the USDA texture triangle. Hundreds of specimens were prepared for each type (sand, silt, and clay). Reduction in soil texture analysis time was achieved using an automatic analysis system. The proposed model detected the texture with an accuracy of up to 99.5% [8].
- The application of portable X-ray fluorescence (PXRF) spectrometry and image analysis was explored to assess soil fertility, organic carbon (OC) availability, Mn, S, and sulfur availability index (SAI) in 1133 soil samples from diverse agroclimatic zones. Color and texture features from soil microscopic images, PXRF data, and soil auxiliary variables (AV) were combined using a random forest model [9].
- Image processing techniques were used to measure the strains generated in flexural tests of reinforced soil beams and to study the propagation of tensile cracks. Adding PET fibers improved the soil response by reducing cracking, increasing tensile strength, and providing ductile behaviour as cracking progressed [10].

- The correlation between the "base color of the soil", the lighting conditions and the corresponding linear regression equation's intersection values is an indicator for predicting the soil components and their water content. This procedure, utilizing digital images from 312 samples [11].
- Micro-CT (High-resolution non-destructive) techniques and two- and three-dimensional image analysis procedures were applied to determine the water retention curve and other hydrological and agricultural functions of compacted and uncompacted sandy soils. These techniques were validated against physical measurements and empirical models. The findings highlight the impact of compaction on soil pore size distribution, water retention capacity and availability, and hydraulic conductivity. The effectiveness of soil characterization using three-dimensional analysis is highlighted [12].
- Four image segmentation methods named “maximum interclass variance (OUST)”, “local adaptive threshold segmentation (LATS)”, “K-means clustering segmentation (KMCS)”, and “natural break point segmentation (NBPS)” were used to process 62 soil images taken with smartphones in sunny and outdoor conditions. The results showed that the methods improved the accuracy in predicting three soil properties (Munsell color, organic matter content and texture) compared to non-segmented images [13].
- The morphometry of the crack pattern on a soil surface was studied using image processing techniques. Samples inoculated with cyanobacteria were evaluated. The results showed that cyanobacterization influences soil crack patterns [14].

The previous literature review identified no recent records regarding the analysis or processing of images in diatomaceous soils. These soils are of importance given their unusual responses and behaviors, which are far from conventional soil mechanics [15][16][17][18][19] [20][21][22]. The state of the art regarding the variation of physical and mechanical properties of soil deposits with the presence of diatom fossils is poorly developed [23]. Conventional geotechnical methods are insufficient to complete SD characterization [24].

Diatomaceous soils (DS) are deposits formed mainly by fossilized remains (amorphous silica) sedimented in bodies of water after the death and organic decomposition of the diatom (algae) [25][26][27]. The frustules (siliceous support structure) can be found as whole or as opalized remains in matrices of clay, organic matter, siltstone, or quartz [28] [29].

Diatom frustules are natural micro- and nanostructured materials generated by biomineralization [30]. They have pores or areoles, various shapes (elongated, spherical, disk), and variable sizes between 10 and 200 μm [31]. These comprise amorphous silica nanospheres deposited in geometric [32] and dimensional patterns depending on the species [30].

This research then contemplated the study of a diatomaceous soil of Colombian origin, whose particles (frustules) present a defined morphological characteristic (cylindrical). In this soil, laboratory tests typical of geotechnical engineering were carried out (unconfined compression, direct shear, oedometric compression), and simultaneously Scanning Electron Microscopy (SEM) images were obtained. Analysis techniques and filters (Binarization, Voronoi, LUT) were applied to these images. This research aims to determine whether, from the images and the results

of mechanical response, some correlation can be established that will later serve as a predictive tool for the behaviour of this type of soil.

Binarization is a digital image processing technique [33], which aims to reduce to two unique tones or values (white: 255 and black: 0); that is, it generates an absence of color. Binarization is achieved by scanning each pixel that forms the image matrix [34][35]. Each pixel is evaluated according to the "sensitivity threshold", a limit that assigns a pure white or black condition above what value is assigned [33]. Binarization optimizes image processing since it reduces the amount of data; each pixel is encoded as 0 or 1 [36].

Voronoi diagram, tessellation or partition is a technique that produces a geometric structure, which divides a space into certain regions, according to the distance to some points called "seeds" or "sites". Each region represents the closest area to a specific seed compared to any other seed in the set [37]. Thiessen polygons (Voronoi diagrams) are used to define and delineate regions close to individual points by using polygonal boundaries [38]. The Voronoi technique is applied in multiple areas, such as geography, computer-aided graphic design [37], meteorology, hydrology and in mining geology to estimate the volumes of exploratory wells, among others [38].

The technique of replacing an image (8, 16, 32 bit) in the simple grey channel with some pseudo color is known as LUT (Look Up Table) [39]. A LUT can be understood as a predefined association (transformation) between grey values with red, green and blue values; with this, the shades of grey can be visualized as colored pixels [40]. A digital image is composed of pixels, and each pixel contains a color. LUTs act as a filter or adjustment formula for the degree of color in each pixel. Look-up table transformations (LUTs) are basic image-processing functions that highlight details in areas that contain important information at the expense of other areas. LUTs apply mathematical formulas to existing colors to change them and achieve the desired result. They adjust gamma, contrast, saturation, luminance and hue, essentially taking the original set of colors and changing them to a new set of colors [41] [42].

MATERIALS AND METHODS

The diatomaceous soil analyzed in this research is of Colombian origin and is of the species Aulacoseira granulata II. See Figure 1. Three states of induced damage, called deterioration cycles (0, 2000 and 4000 DC), were considered for this soil. Likewise, the soil was evaluated under three conditions of gravimetric dosing (33, 66 and 100% DS%) supplemented with a matrix of Kaolin-type clay soil. The soils were prepared artificially under a pre-consolidation stress of 100 kPa.

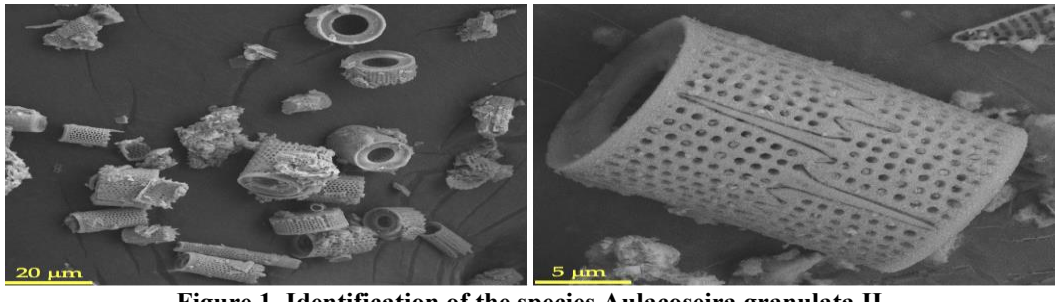

Figure 1. Identification of the species Aulacoseira granulata II

Samples were taken from each of the soil mixtures for direct shear, unconfined compression and oedometric compression tests. The test conditions are summarized in Table 1.

Test type	Test feature		
Direct Shear	Sample height	cm	2.46
	Sample area	cm^2	20.15
	Shear box type	---	circular
	Normal Stress	kg/cm^2	"1 - 4"
	Beam ratio	---	10
Unconfined Compression	Sample diameter	cm	5.98-6.07
	Sample height	cm	11.90 - 12.81
	Strain velocity	mm/min	1.20 - 2.56
	Moisture	%	46.21 - 123.78
Oedometric compression	Specific gravity	---	2.29 - 2.61
	Beam ratio	---	10
	Wet density	g/cm^3	1.29 - 1.70
	Dry density	g/cm^3	0.58 - 1.14
	Sample volume	cm^3	39.27

Table 1. Conditions for performing laboratory tests.

Samples were taken and observed for each dosing and deterioration condition using a Scanning Electron Microscope (SEM). This equipment is a Carl Zeiss Evo HD 15, with a LaB6 (lanthanum hexaboride) emitter and Smart SEM software version 5.07. The sample metallizer is a Quorum Q150R ES reference. See Figure 2. The observed samples come from the unconfined compression specimens after their failure.

The SEM study considered a range of zooms between 200X-6400X. The condition selected for the comparative analysis was 1600X. Once the images were defined, they were processed using ImageJ 1.53 software. In this system, the simple binarization, Voronoi and Red-Green filter techniques were applied. The scale was set for each image, and the treatment was done on duplicates. The particularities of each technique are explained as follows:

- **Simple binarization:** (Process>Binary>Make Binary) 8-bit image. See Figure 3a.
- **Voronoi**: (Process>Binary> Make Binary >No fill holes>Voronoi) 8-bit binarized image. “No fill holes” condition. For visualization purposes, the criteria for Brightness (40%), Contrast (-40%), Saturation (100%) and Temperature (1517) were adjusted. See Figure 3b.
- **Red-Green LUT:** 8-bit image. Three numbering limits 100,125, and 150, were evaluated. Figure 3c.

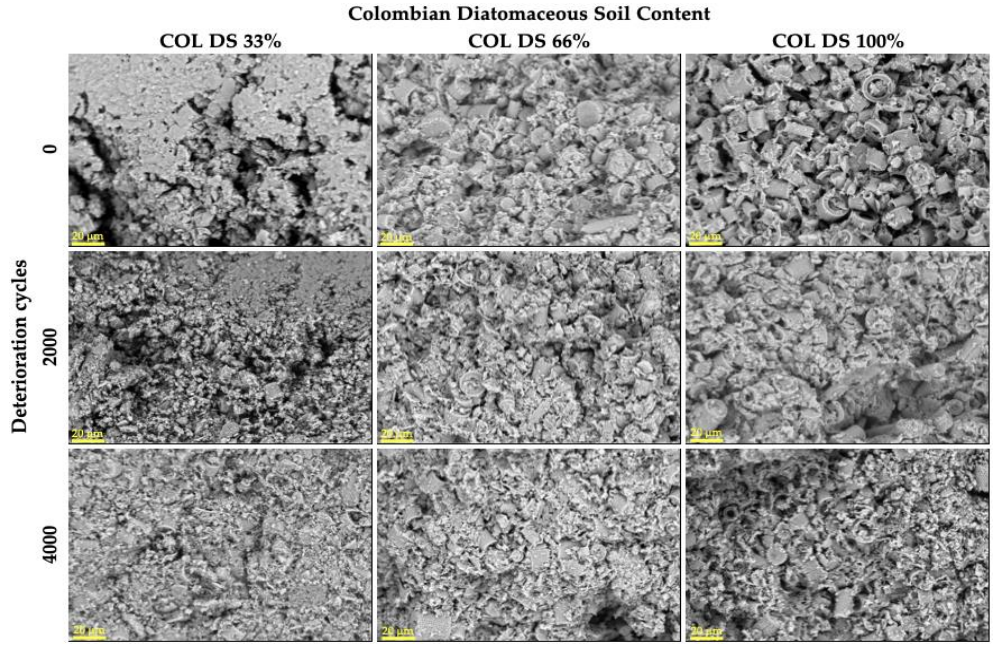

Figure 2. SEM record of diatomaceous soil according to study variables.

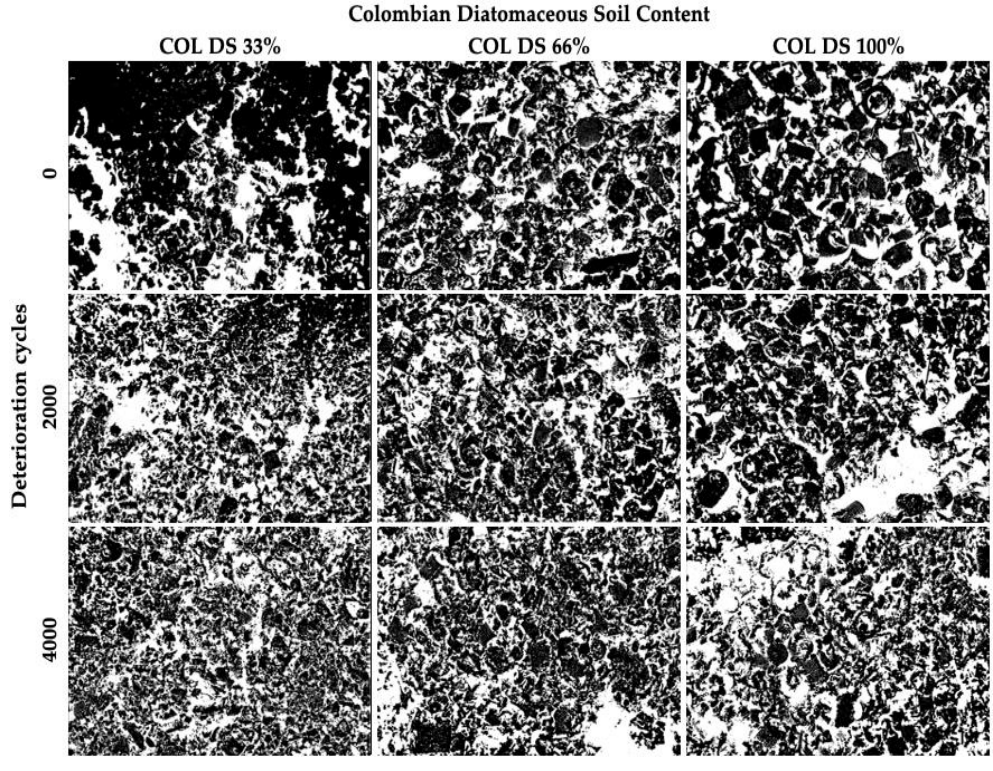

Figure 3a. SEM image representation with application of simple Binarization technique.

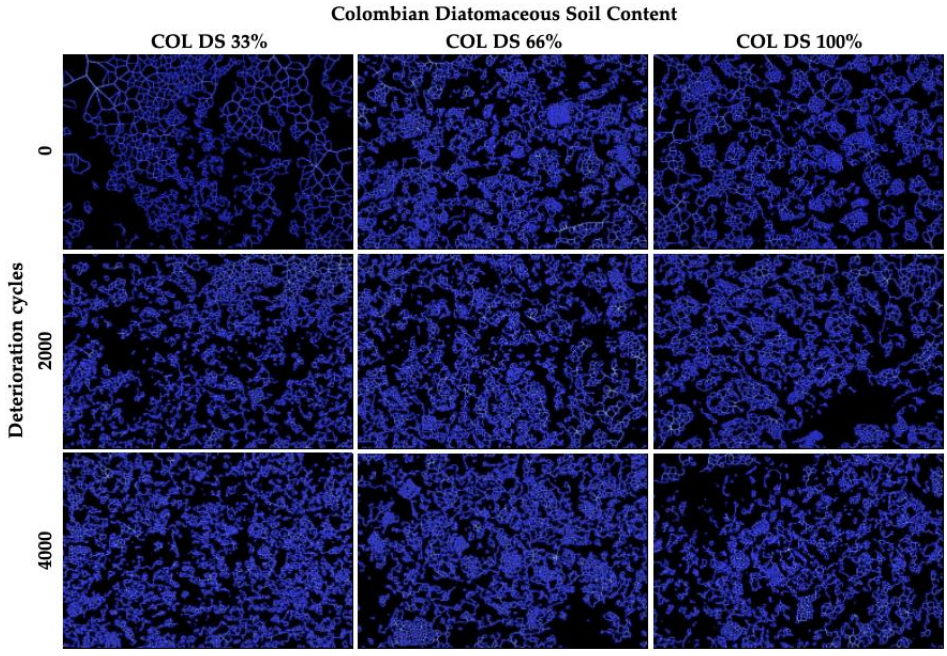

Figure 3b. SEM image representation with the application of the VORONOI technique.

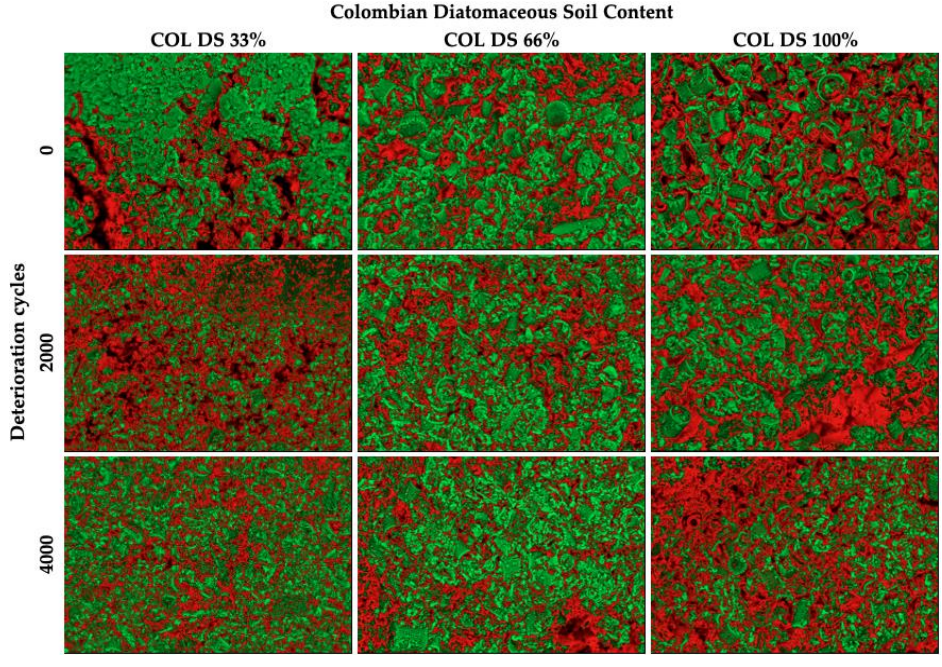

Figure 3c. SEM image representation with "Red-Green LUT" application.

Once the results of each technique for each dosage condition and deterioration level were obtained (figure 3a, 3b, 3c), quantification methods were proposed that could be compared with the laboratory results (Direct Shear, Unconfined Compression, Oedometric Compression) and formulations were projected that would allow relating the results of the processed SEM image

with the results of the laboratory test, that is, it was proposed that from a microscopy image the values of some parameters obtained in the physical tests could be determined. The conditions that showed more promising numerical compatibility between the processed SEM photograph and the physical laboratory tests are shown in table 2.

Image Processing Method	Physical parameter	Laboratory test
Binary	Final void ratio	Oedometric compression
Binary	Cohesion	Direct shear
Green-Red LUT _ pixel limit 100	Failure strain	Unconfined Compression
Voronoi _ "No fill Holes" condition	Cohesion	Direct shear

Table 2. Methods and related physical parameters

Results and Discussion

First, the consolidated results of the geotechnical assessment for the soil are presented based on the study variables, diatomaceous soil content (DS%), and deterioration cycles (DC). See Figure 4. Next, Figure 5 presents some trends between the results of the different tests, identifying proportional behaviors described almost by a linear condition.

The friction angle varies between 23° (DS 100% - 0 DC) and 37° (DS 33% - 4000 DC). The maximum value (37°) is typical of granular soils (sands or gravel) and not so much of fine soils (silts), such as diatomaceous soils. This peak value is striking since the concentration of fossils was only 33%, but the number of deterioration cycles was the highest (4000); that is, fracturing the frustules had the greatest impact and not so much their concentration in the soil mixture.

The void ratio increases with the higher fossil content (a situation expected due to micro and nano pores). The greater the number of deterioration cycles, the lower the voids are due to the breakdown of the microstructures (collapse of the cylindrical shape of the fossil). The highest void ratio value (3.14) is associated with a sample with 100% DS and no deterioration cycles. On the other hand, the lowest void ratio (1.32) is associated with the sample with the highest fine matrix content and the highest level of fossil deterioration. This behavior was expected. Even the lowest value (1.32) is extensive compared to typical void ratio records in other fine soils.

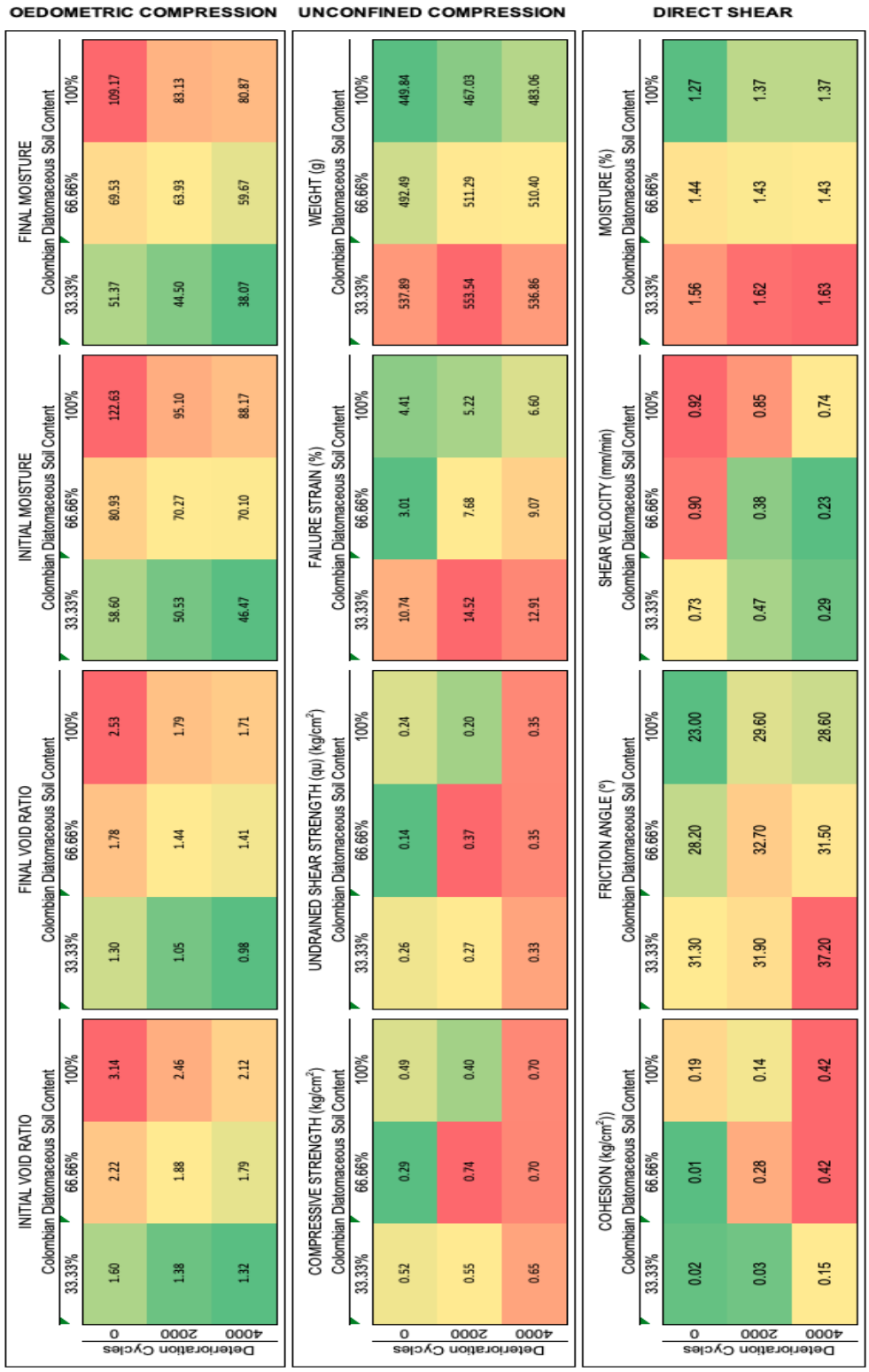

Figure 4. Consolidated record of laboratory test results.

The wet unit weight decreases with the highest fossil content and with the lowest number of deterioration cycles (lower soil densification due to the cylindrical structure). The lowest value (1.27 g/cm^3) is associated with a concentration of 100% DS and no deterioration cycles. The highest value (1.63 g/cm^3) is related to the highest number of cycles (4000 DC) and lowest concentration (33% DS).

An increase in failure strain is observed as the sample becomes denser (lower void ratio and higher unit weight); a denser sample is expected to support a higher load level before reaching its failure point. A lower deformation at failure is recognized with a lower fossil content and fewer deterioration cycles.

Similar to conventional soil, an increase in the friction angle is observed with the decrease in the void ratio and with the increase in unit weight. On the other hand, a higher peak strain (unconfined compression failure criterion) is observed when the sample is densified, represented by a lower void ratio and a higher wet unit weight.

In all cases, it is observed that the effects of the relationship between parameters become more intense as the number of deterioration cycles increases. Conversely, and for any level of deterioration (0, 2000 or 4000 cycles), it is observed that the effects increase with the decrease in the concentration of diatomaceous soils. See figure 5.

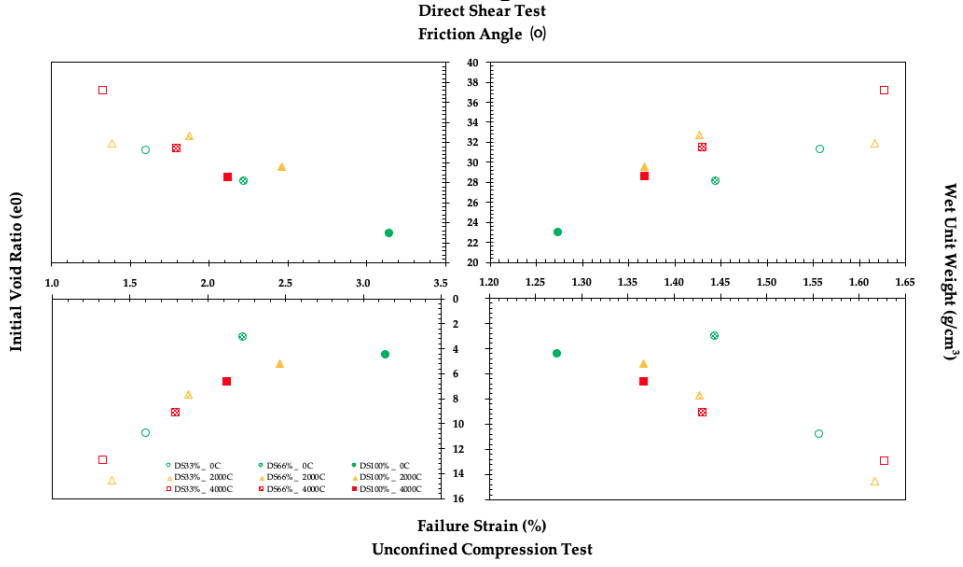

Figure 5. Relationship of multi-test criteria in diatomaceous soil.

Figure 6 presents the results of the physical test of final void ratio, cohesion (kg/cm^2), and strain at failure (%) (Column A) and those calculated from image analysis (Column B), both based on the study variables (deterioration cycles and frustule concentration). The numerical closeness in orders of magnitude and the similarity of behavior of the parameters evaluated based on the study variables are denoted.

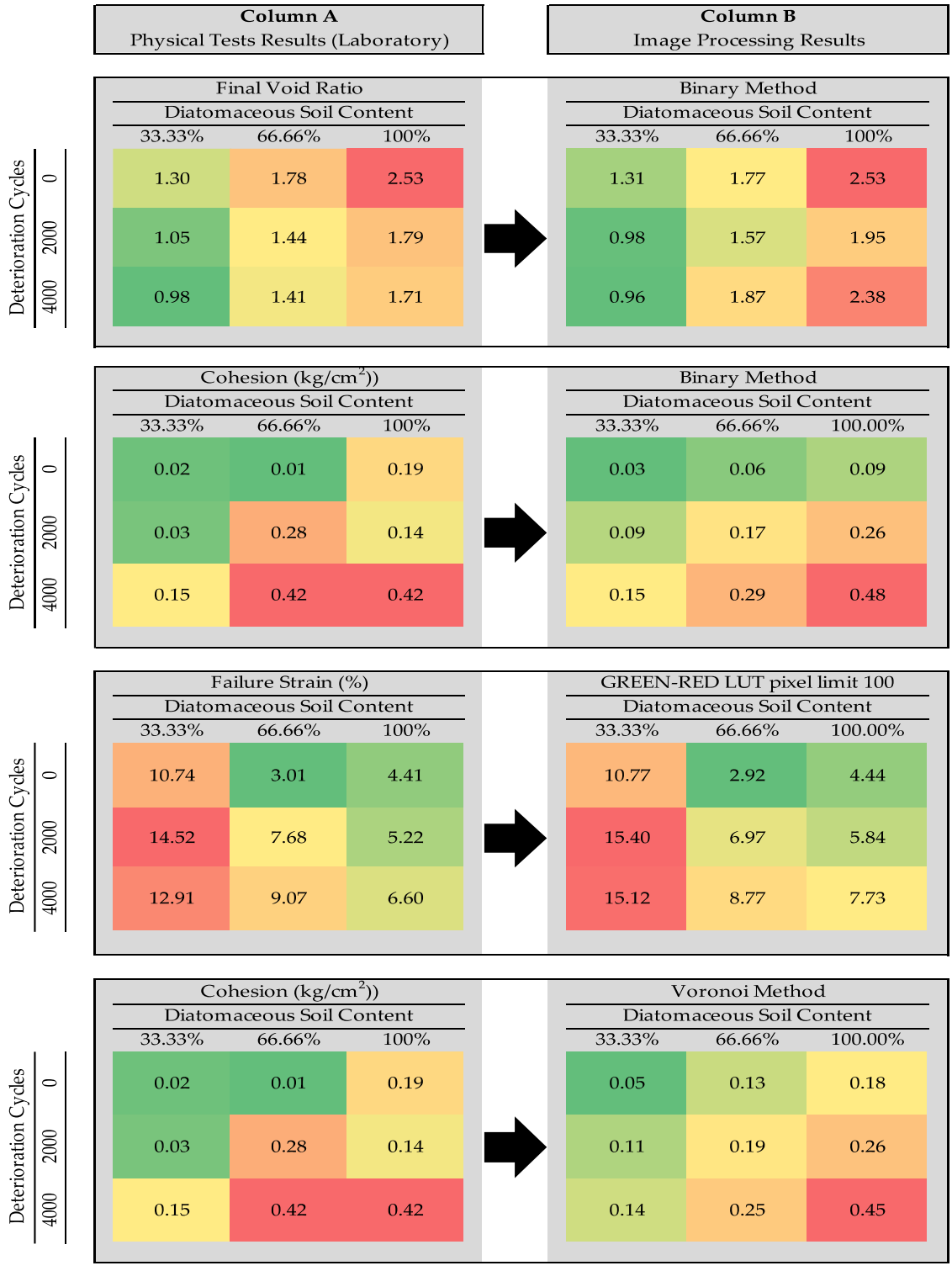

Figure 6. Relationship of results obtained between laboratory tests and image processing.

Table 3 presents the formulations through which the study's physical parameters were obtained, based on the results of each processing technique, level of deterioration, and concentration of frustules.

Image Processing Method	Physical parameter	Symbol
Binary	Final Void Ratio	e
$e = \frac{100*DS\%}{B} + \left(\left((2 \times 10^{-7} * DC^2) - (7 \times 10^{-4} * DC) - 0.4863\right) * DS\%\right) + \left((-7 \times 10^{-8} * DC^2) + (3 \times 10^{-4} * DC) + 0.42\right) - \left(\frac{3600*DC}{DS\%}\right)$ (1).		
B= (∑ pixels Value / 255) / Image Area in pixels. DS%: Diatomaceous Soil Content. DC: Deterioration Cycles.		

Image Processing Method	Physical parameter	Symbol
Binary	Cohesion	C
$C = \frac{B}{100} * \left(2 \times 10^{-4} * \left((0.1 + DC) * DS\%\right) + 0.02)\right) + \left((0.08 * 1^{DC}) * DS\%\right)$ (2).		

Image Processing Method	Physical parameter	Symbol
Green-Red LUT pixel limit 100	Failure Strain	D_f
$Df = \frac{GR}{2.55} - \left((3 \times 10^{-6} * DC^2) - (0.0102 * DC) + 13.003) * DS\%\right) + ((-2 \times 10^{-6} * DC^2) + (0.0058 * DC) - 5.65)$ (3).		
GR= ∑ pixel values limited to 100 / Image Area in pixels.		

Image Processing Method	Physical parameter	Symbol
Voronoi condition "No fill Holes"	Cohesion	C
$C = \frac{100000*DS\%}{VOR} * (0.0001 * DC + 0.66)$ (4).		
VOR= ∑ pixels values Voronoi filter.		

Bibliography

Y. Wu, J. Yan, Y. Zhang, Y. Kong, and Z. Song, "Combination of digital image processing and random generation in modeling soil-rock mixture slopes for post-failure analyses by material point method," *Comput. Geotech.*, vol. 165, no. August 2023, p. 105886, 2024, doi: 10.1016/j.compgeo.2023.105886.

Y. Zhou, A. Biswas, Y. Hong, S. Chen, B. Hu, and Z. Shi, "Geoderma Enhancing soil profile

analysis with soil spectral libraries and laboratory hyperspectral imaging," *Geoderma*, vol. 450, no. May, p. 117036, 2024, doi: 10.1016/j.geoderma.2024.117036.

G. Liu, S. Tian, Q. Wang, H. Wang, and L. Kong, "High-resolution measurement of moisture filed at soil surface with interfered image processing method and machine learning techniques," *J. Hydrol.*, vol. 652, no. July 2024, p. 132623, 2025, doi: 10.1016/j.jhydrol.2024.132623.

H. Li, X. Gong, and B. Shi, "Tensile strength of clayey soil and the strain analysis based on image processing techniques," vol. 253, no. April, pp. 1–8, 2019.

L. Gao, D. Wang, and Y. Miao, "A review of two-dimensional image-based technologies for size and shape characterization of coarse-grained granular soils," *Powder Technol.*, vol. 445, no. June, p. 120115, 2024, doi: 10.1016/j.powtec.2024.120115.

M. K. Vakilzadeh Ebrahimi, H. Lee, J. Won, S. Kim, and S. S. Park, "Estimation of soil texture by fusion of near-infrared spectroscopy and image data based on convolutional neural network," *Comput. Electron. Agric.*, vol. 212, no. February, p. 108117, 2023, doi: 10.1016/j.compag.2023.108117.

M. Naeimi, P. Daggupati, and A. Biswas, "Image-based soil characterization: A review on smartphone applications," *Comput. Electron. Agric.*, vol. 227, no. P1, p. 109502, 2024, doi: 10.1016/j.compag.2024.109502.

K. Sattar *et al.*, "Soil texture analysis using controlled image processing," *Smart Agric. Technol.*, vol. 9, no. August, p. 100588, 2024, doi: 10.1016/j.atech.2024.100588.

S. Dasgupta *et al.*, "Soil fertility prediction using combined USB-microscope based soil image, auxiliary variables, and portable X-ray fluorescence spectrometry," *Soil Adv.*, vol. 2, no. June, p. 100016, 2024, doi: 10.1016/j.soilad.2024.100016.

C. Hernández, E. Botero, and G. Beltrán, "The study of fracture mechanics of PET fiber-reinforced soils based on flexural tests and imaging techniques," *Transp. Geotech.*, vol. 51, p. 101486, 2025, doi: 10.1016/j.trgeo.2025.101486.

[11] S. Baek, J. Jeon, and T. Kwak, "Prediction of Soil Composition Using Digital Images Taken under Variable Lighting Environments," *KSCE J. Civ. Eng.*, p. 100093, 2024, doi: 10.1016/j.kscej.2024.100093.

N. Goldberg-Yehuda, U. Nachshon, S. Assouline, and Y. Mau, "The effect of mechanical compaction on the soil water retention curve: Insights from a rapid image analysis of micro-CT scanning," *Catena*, vol. 242, no. May, p. 108068, 2024, doi: 10.1016/j.catena.2024.108068.

J. Yang, T. Wang, Y. Liang, and Y. Wei, "Image segmentation and dominant region feature extraction for original soil: Towards soil property prediction based on images acquired from smartphones," *Catena*, vol. 233, no. March, p. 107508, 2023, doi: 10.1016/j.catena.2023.107508.

S. Gharemahmudli, S. H. Sadeghi, V. S. Sadeghi, A. Najafinejad, and A. Jafarpoor, "Morphometrical analysis of cracks and crevices on a cyanobacterized soil surface subjected to a freeze-thaw cycle using image processing," *Catena*, vol. 213, no. February, p. 106150, 2022, doi: 10.1016/j.catena.2022.106150.

J. Locat and H. Tanaka, "A new class of soils: fossiliferous soils?," in *XV International Conference of Soil Mechanics and Geotechnical Engineering*, 2001, pp. 2295–2300.

J. C. Ruge, W. Castro, J. Camacho, and F. Molina, "Dependencia de las propiedades de retención de agua en suelos caoliníticos con contenidos de microalgas fosilizadas adicionadas artificialmente," in *Geotechnical Engineering in the XXI Century: Lessons learned and*

future challenges, 2019, pp. 780–787, doi: 10.3233/STAL190112.
G. Arenaldi, C. Ovalle, and A. Barrios, "Compressibility and creep of a diatomaceous soil," *Eng. Geol.*, vol. 258, no. May, p. 105145, 2019, doi: 10.1016/j.enggeo.2019.105145.
B. Caicedo, C. Mendoza, F. López, and A. Lizcano, "Behavior of diatomaceous soil in lacustrine deposits of Bogotá, Colombia," *J. Rock Mech. Geotech. Eng.*, vol. 10, no. 2, pp. 367–379, 2018, doi: 10.1016/j.jrmge.2017.10.005.
A. M. Palomino, S. Kim, A. Summitt, and D. Fratta, "Impact of diatoms on fabric and chemical stability of diatom-kaolin mixtures," *Appl. Clay Sci.*, vol. 51, no. 3, pp. 287–294, 2011, doi: 10.1016/j.clay.2010.12.002.
Q. Su, Z. Deng, X. Wang, W. Jia, and Y. Niu, "Experimental Study of the Dynamic Characteristics of a New Antidrainage Subgrade Structure for High-Speed Railways in Diatomaceous Earth Areas," *Materials (Basel).*, vol. 15, no. 2, 2022, doi: 10.3390/ma15020532.
C. Ovalle and G. Arenaldi, "Mechanical behaviour of undisturbed diatomaceous soil," *Mar. Georesources Geotechnol.*, vol. 39, no. 5, pp. 623–630, 2020, doi: 10.1080/1064119X.2020.1720049.
J. L. Qu and D. X. Zhao, "Comparative research on tillable properties of diatomite-improved soils in the Yangtze River Delta region, China," *Sci. Total Environ.*, vol. 568, pp. 480–488, 2016, doi: 10.1016/j.scitotenv.2016.06.056.
A. Covarrubias, J. Wang, D. Moug, M. Evans, and A. Walter, "Geo-Congress 2022 ASCE," in *Relating the Proportion of Diatom Particles to the Physical Properties of Natural Diatomaceous Soil*, 2022, pp. 479–489, [Online]. Available: https://ascelibrary.org/doi/abs/10.1061/9780784484036.047.
G. Wiemer *et al.*, "The role of sediment composition and behavior under dynamic loading conditions on slope failure initiation: a study of a subaqueous landslide in earthquake-prone South-Central Chile," *Int. J. Earth Sci.*, vol. 104, no. 5, pp. 1439–1457, 2015, doi: 10.1007/s00531-015-1144-8.
G. Arenaldi and C. Ovalle, "Compresibilidad y propiedades dinámicas de suelos diatomáceos de Mejillones Compressibility and dynamic properties of diatomaceous soils of Mejillones Introducción Sector de estudio Material de ensayo," *Obras y Proy.*, vol. 25, pp. 6–14, 2019.
J. M. Mejía, R. Mejía De Gutiérrez, and C. Montes, "Rice husk ash and spent diatomaceous earth as a source of silica to fabricate a geopolymeric binary binder," *J. Clean. Prod.*, vol. 118, pp. 133–139, 2016, doi: 10.1016/j.jclepro.2016.01.057.
R. J. Flower, *Diatomites: Their Formation, Distribution, and Uses*, 2nd ed. Elsevier B.V., 2013.
Agropuli, "Ficha técnica 'TIERRA DE DIATOMEAS - AGROPULÍ - TDDA Silicio asimilable: dióxido de silicio (SiO2) amorfo. Enmienda de uso agrícola.'" Bogotá, pp. 1–13, 2021.
B. L. E. Antonides, "Diatomites," *US Geological Survey Publications*. 1997.
A. Rogato and E. De Tommasi, "Physical , Chemical , and Genetic Techniques for Diatom Frustule Modification : Applications in Nanotechnology," *Appl. Sci.*, vol. 10, no. 8738, pp. 1–23, 2020, doi: 10.3390/app10238738.
H. Al Shatnawi and P. Bandini, "Oedometric Behavior of a Diatom-Kaolin Mixture," in *Geo-Congress 2019*, 2019, pp. 673–681.
Z. V. Finkel and B. Kotrc, "Silica use through time: Macroevolutionary change in the morphology of the diatom fustule," *Geomicrobiol. J.*, vol. 27, no. 6–7, pp. 596–608, 2010, doi: 10.1080/01490451003702941.

E. Molina, J. Diaz, H. Hidalgo, and E. Chávez, "Algoritmos de Binarización Robusta de Imágenes con Iluminación No Uniforme," *Rev. Iberoam. Automática e Informática Ind.*, vol. 15, pp. 252–261, 2018, doi: https://doi.org/10.4995/riai.2017.8847.

R. Magro, "BINARIZACIÓN DE IMÁGENES DIGITALES Y SU ALGORITMIA COMO HERRAMIENTA APLICADA A LA ILUSTRACIÓN ENTOMOLÓGICA," *Boletín la Soc. Entomológica Aragon.*, vol. 53, no. 1, pp. 443–464, 2013.

F. Cortés, "Binarización de una imagen," *Blog de programacion para estudiantes.*, 2014. https://cortesfernando.blogspot.com/2014/05/binarizacion-imagen.html.

E. De la Fuente and F. Trespaderne, "Visión Artificial Industrial," Valladolid, 2013.

geeksforgeeks, "Voronoi Diagram," 2014. https://www.geeksforgeeks.org/voronoi-diagram/ (accessed Jan. 20, 2024).

B. Harrison, "9.11 Thiessen polygon mapping," in *Data room management for mergers and acquisitions in the Oil and Gas Industry*, Elsevier, Ed. Elsevier, 2020, pp. 145–167.

Universidad del País Vasco - sgiker, "Cambio de color (LUT) de imágenes en blanco y negro en Image J." 2024, [Online]. Available: http://www.ehu.es/SGIker.

ImageJ.net, "Image Processing and Analysis in Java," 2025. https://imagej.net/ij/download/luts/.

Vegas Creative Software, "What are and how use luts in color grading," *Types of LUTs*, 2025. https://www.vegascreativesoftware.com/us/video-editing/what-are-and-how-use-luts-in-color-grading/#:~:text=LUTs (Lookup Tables) are a,and achieve a desired result.

WISTIA, "What is a LUT? How to Use LUTs for Color Grading," *What is a LUT? How to Use LUTs for Color Grading*, 2022. https://wistia.com/learn/production/how-to-use-luts-for-color-grading#:~:text=A digital image is made,grade-preset for your footage.